

Observation of a Tunable Isolated Dirac Point in $\text{Ge}(\text{Bi}_x\text{Sb}_{1-x})_2\text{Te}_4$

Sean Howard¹, Arjun Raghavan¹, Davide Iaia¹, Caizhi Xu¹, David Flötotto¹, Man-Hong Wong¹, Sung-Kwan Mo², Bahadur Singh³, Raman Sankar⁴, Hsin Lin⁴, Tai-Chang Chiang¹, and Vidya Madhavan^{1*}

1. Department of Physics and Frederick Seitz Materials Research Laboratory, University of Illinois at Urbana-Champaign, Urbana, IL, USA
2. Advanced Light Source, Lawrence Berkeley National Laboratory, Berkeley, CA, USA
3. Department of Condensed Matter Physics and Materials Science, Tata Institute of Fundamental Research, Mumbai 400005, India
4. Institute of Physics, Academia Sinica, Taipei, Taiwan 11529

[*vm1@illinois.edu](mailto:vm1@illinois.edu)

Abstract

Novel topological devices require the isolation of topological surface states from trivial bulk states for electronic transport¹⁻³. In this study, we examine a tunable topological system, $\text{Ge}(\text{Bi}_x\text{Sb}_{1-x})_2\text{Te}_4$, for a range of x values, using a combination of Fourier Transform Scanning Tunneling Spectroscopy (FT-STs) and Angle-Resolved Photoemission Spectroscopy (ARPES). We track the evolution of the bulk and surface state band structure for different values of x from 1 to 0.4. Our results show that the system remains topologically non-trivial down to $x = 0.4$, extending the range predicted by previous computational studies⁴. Importantly, we find that the Dirac point crosses the Fermi energy near $x = 0.65$. Our observation of a tunable Dirac point which crosses into the topological transport regime can be important for topological spintronics applications⁵.

Introduction

Since the discovery of topological materials, much effort has been made to utilize the properties of topologically protected states in novel electronic devices^{6,7}. Among the primary challenges in realizing such devices is the isolation of topological surface states from a background of trivial bulk states¹⁻³. If the chemical potential intersects bulk valence or conduction bands, transport will be dominated by bulk contributions⁸. To avoid this, the chemical potential must be manipulated into the band gap containing topological states, while keeping the band topology non-trivial.

One method to achieve transport dominated by topological states is chemical substitution. This type of topological engineering has been previously studied in material systems including $\text{Bi}_{2-x}\text{Sb}_x\text{Te}_{3-y}\text{Se}_y$, $(\text{Bi}_{1-x}\text{Sb}_x)_2\text{Te}_3$, and $\text{BiTI}(\text{S}_{1-x}\text{Se}_x)_2$ ⁹⁻¹¹. In these materials, substitution moves the system into the topological transport regime, where transport is dominated by spin polarized topological states^{9,11}. However, the systems previously studied have several challenges¹² associated with them, including difficulty in growth of materials and the lack of an isolated Dirac point. This motivates the study of new materials for topological engineering, and one such system is $\text{Ge}(\text{Bi}_x\text{Sb}_{1-x})_2\text{Te}_4$.

Several properties of $\text{Ge}(\text{Bi}_x\text{Sb}_{1-x})_2\text{Te}_4$ suggest the potential for tuning its topological states by substitution, making it ideal for optimizing the band structure to achieve transport dominated by the topological bands. Of the two parent compounds, GeBi_2Te_4 and GeSb_2Te_4 , of this system, GeBi_2Te_4 is known to be a topological insulator with a band gap of ≈ 200 meV and an isolated Dirac point 280 meV below the Fermi energy¹³. This is advantageous since an isolated Dirac point is a critical component of electrical transport dominated by topological surface states (TSS). Moreover, calculations⁴ predict a topologically non-trivial to trivial transition between $x = 0.5$ and $x = 0.6$, further suggesting the potential tunability of $\text{Ge}(\text{Bi}_x\text{Sb}_{1-x})_2\text{Te}_4$.

Other material properties also contribute to technological interest in the system. Both parent compounds of this system are known thermoelectric materials¹⁴. In addition, GeSb_2Te_4 is a phase change material which enters a metastable rock-salt phase by rapid cooling, suggesting possible use in nonvolatile random-access memory devices^{15,16}. Finally, a large spin polarization is measured in the TSS of GeBi_2Te_4 by spin-resolved ARPES¹⁷, which can be important for increased efficiency of spintronics devices. Detailed experimental studies of the effects of substitution in $\text{Ge}(\text{Bi}_x\text{Sb}_{1-x})_2\text{Te}_4$ are therefore critically needed to understand its potential utility in a variety of electronic and spintronic applications.

Experimental Methods

In this work, a combination of Fourier Transform Scanning Tunneling Microscopy (FT-STs) and Angle-Resolved Photoemission Spectroscopy (ARPES) is used to investigate $\text{Ge}(\text{Bi}_x\text{Sb}_{1-x})_2\text{Te}_4$. ARPES measurements were carried out at the BL 10.0.1, Advanced Light Source, Lawrence Berkeley National Laboratory. To investigate the band structure of unoccupied states above the Fermi energy, and to confirm ARPES results

below the Fermi energy, FT-STs is used. FT-STs measurements are performed at 4 K with a scanning tunneling microscope (STM) in ultrahigh vacuum; bulk single crystals are cleaved *in situ* and measured with annealed W STM tips. Details of crystal growth are given in the Appendix.

The FT-STs technique utilizes quasiparticle interference (QPI) in the system, occurring due to quasiparticle scattering from defects and other imperfections, and yielding energy-dependent standing waves¹⁸. While direct backscattering is in general prohibited for topological surface states, due to the effects of hexagonal warping, a significant QPI signal is generated in $\text{Ge}(\text{Bi}_x\text{Sb}_{1-x})_2\text{Te}_4$ ^{12,19,20}. These warping effects have been previously observed in Bi_2Te_3 ²⁰ and GeBi_2Te_4 ²¹, for example. Using the measured QPI scattering vectors, momentum-space band structure information is obtained. The combination of FT-STs and ARPES thus provides a powerful means to understand changes in the topological properties of the $\text{Ge}(\text{Bi}_x\text{Sb}_{1-x})_2\text{Te}_4$ system.

Results and Discussion

$\text{Ge}(\text{Bi}_x\text{Sb}_{1-x})_2\text{Te}_4$ crystals consist of stacked hexagonal layers forming a unit cell with $c = 41.3 \text{ \AA}$ ²², as shown in Fig. 1(a). Previous density functional theory (DFT) calculations of the system performed by Singh, et al. (2013) predict a trivial to topologically non-trivial phase transition as Bi substitution is increased above $x = 0.55$ ⁴. Fig. 1(b) shows the calculated closing and reopening of a bulk gap with inverted band order involved in the transition. As given schematically in Fig. 1(c), the appearance of gapless topological surface states accompanies the reopening of this bulk gap.

To characterize the surface, we obtain STM images of the cleaved crystals. Cleavage occurs between van der Waals bonded Te layers, as indicated in Fig. 1(a). A typical STM topography scan obtained on the parent GeBi_2Te_4 shows the hexagonal lattice expected for these surfaces (Fig. 1(d)). While the hexagonal structure is clear, it is evident that the surface is electronically inhomogeneous. This is, however, not unexpected given that the system is known to be prone to disorder^{23,24}. Fig. 1(e) shows STM dI/dV spectra, representing the local density of states (LDOS), for substitutions $x = 0.6$ and $x = 1.0$. The spectra are found to have major differences in locations of their minima and gap size. These are indicative of significant changes in the band structure due to substitution, and motivate further investigation using ARPES and FT-STs. For a first estimate, the Dirac point can be approximated²⁵ as the minimum of a dI/dV spectrum. For $x = 1.0$, the minimum occurs near -270 meV , in agreement with the -280 meV ARPES measurement²¹ by Arita, et al. (2014). With $x = 0.6$, we find the spectrum to have a minimum above zero bias, suggesting that Sb substitution has caused the Dirac point to cross the Fermi energy.

We next measure the band structure of $\text{Ge}(\text{Bi}_x\text{Sb}_{1-x})_2\text{Te}_4$ for the compositions $x = 1, 0.7, 0.6, 0.5$, and 0.4 using ARPES. Fig. 2(a) shows ARPES data for $x = 1$, that is, GeBi_2Te_4 , along the Γ -K direction. The intensity below a binding energy of 0.6 eV is from the bulk valence band. We also observe the contribution from the conduction band near

the chemical potential. Surface states with approximate linear dispersion are seen to cross at a Dirac point near the zone center. The dispersion for substitutions $\text{Ge}(\text{Bi}_x\text{Sb}_{1-x})_2\text{Te}_4$ from $x = 0.7$, down to $x = 0.4$, are shown in Fig. 2(b)-(e). At all compositions, we observe the presence of quasi-linearly dispersing in-gap states. We confirm that the in-gap states seen are 2-dimensional surface states by varying the incoming photon energy. As demonstrated for $\text{GeBi}_{1.4}\text{Sb}_{0.6}\text{Te}_4$ in Fig. 2(f)-(h), with changing photon energy, the in-gap states remain unchanged, while there are clear changes in the bulk valence bands at higher binding energies.

The data show that with decreasing x , the Dirac point crosses the Fermi level (E_F) around a composition of $x = 0.65$, though the dispersion as well as the exact location of the Dirac point are hard to ascertain. To obtain further insights into the evolution of the band structure with Sb substitution, we shift the relative position of E_F by depositing potassium on the surface (Fig. 2(i)-(j)). Using this data, we can obtain the relative position of the Dirac point with increasing Sb substitution. The results are shown in Fig. 3(g). ARPES results thus provide valuable information on changes in Dirac point energy with Sb substitution and confirm the presence of topological surface states.

For comparison with and corroboration of the ARPES data, FT-STs quasiparticle interference (QPI) scattering is employed. At $x = 0.6-1.0$, detailed local density of states (LDOS) maps over a range of more than 800 meV in energy are measured. Sample LDOS maps in $\text{GeBi}_{1.4}\text{Sb}_{0.6}\text{Te}_4$ at -50 meV and 100 meV, of size 60 nm \times 60 nm, are shown in Fig. 3(a)-(b). We perform Fourier Transforms of each of these maps for analysis. In $\text{Ge}(\text{Bi}_x\text{Sb}_{1-x})_2\text{Te}_4$, scattering between the hexagonally warped surface bands yields a significant QPI signal²⁰. Due to the spin texture, the signal is dominated by scattering across vectors connecting Γ -K bands, resulting in scattering vectors along the Bragg peak Γ -M direction²⁰; this scattering geometry is shown in Fig. 3(c). Based on this geometry, reciprocal space \mathbf{k} momentum vectors measured by ARPES relate to measured QPI scattering vectors \mathbf{Q} by $\mathbf{Q} = \sqrt{3}\mathbf{k}$. In Fig. 3(d)-(e), the Fourier transforms of the LDOS maps at -50 meV and 100 meV are presented. The Bragg peaks are faintly visible at the corners of the FTs, and it is clear that the scattering wavevectors occur only in these Γ -M directions. Moreover, a significant change in the wavevectors is seen as a function of energy: as the energy is increased, the wavevectors get larger, indicating positive dispersion.

For quantitative analysis, we plot full energy-momentum dispersions from FT-STs data at $x = 0.6, 0.7$, and 1.0 in Fig. 3(f). To obtain estimates of the Dirac point from FT-STs, the low-energy dispersion from ARPES data shown in Fig. 2(a) is applied to the present QPI data²⁴. Specifically, the ARPES dispersion of the $x = 1$ compound (thick solid line in Fig. 3(f)) is simply shifted rigidly to match the dispersion curves from FT-STs. From this analysis, we can estimate that the Dirac points occur at energy values of -320 meV, -140 meV, and 40 meV for $x = 1.0, 0.7$, and 0.6 , respectively.

We can now compare data from the FT-STs and ARPES measurements. The Dirac point energy is shown to vary approximately linearly with doping in both data sets,

as seen in Fig. 3(g). Values of these energies agree well between the two techniques. Our most significant conclusion is that the Dirac point of the system crosses above the Fermi energy and into the topological transport regime for $x < 0.65$, which is a very important feature for spintronic applications⁵. In addition, ARPES measurements suggest that the system remains topological down to at least $x = 0.4$, extending the range predicted⁴ by DFT.

Conclusion

In conclusion, this combined ARPES and FT-STs study has experimentally revealed a novel tunable topological insulator system, $\text{Ge}(\text{Bi}_x\text{Sb}_{1-x})_2\text{Te}_4$. The ability to tune the Dirac point to cross the Fermi energy by substitution will allow for new topological transport applications for this material system, especially due to its well-isolated Dirac point. In the current work, we have also extended the bounds of the topological regime predicted⁴ by theory. Differences between previous DFT calculations⁴ and present experimental measurements may be due to the existence of disorder, as is directly visualized in the STM topographies. Future work utilizing Landau level spectroscopy²⁶ can elucidate the precise location of the expected trivial-to-topological phase transition. The topology of $\text{Ge}(\text{Bi}_x\text{Sb}_{1-x})_2\text{Te}_4$ thus provides a unique platform for a number of novel fundamental studies and technological applications.

Appendix

The highly oriented single crystals of $\text{Ge}(\text{Bi}_x\text{Sb}_{1-x})_2\text{Te}_4$ are grown by using the vertical Bridgman method. Initially, stoichiometric mixtures of $\text{Ge}(\text{Bi}_x\text{Sb}_{1-x})_2\text{Te}_4$ compounds were prepared with high purity metal precursors (5N) of bismuth (Bi), antimony (Sb), germanium (Ge) and tellurium (Te). These initial powders of $\text{Ge}(\text{Bi}_x\text{Sb}_{1-x})_2\text{Te}_4$ were calcinated at 800 °C for 24 hrs. in a crucible furnace and then cooled down to room temperature slowly. Further finely ground compounds were transferred in carbon coated quartz tubes for highly oriented single crystal growth under an Ar atmosphere purged environment and sealed under a vacuum of $\approx 2 \times 10^{-3}$ Torr. These double sealed quartz tubes powders were then heated at 900 °C for 200 hrs. in a vertical Bridgman furnace to grow single crystals. The schematic of the crystal growth setup is shown in the inset of Fig. A.1. A temperature gradient of ≈ 0.5 °C/mm is programmed at near the solidification point (marked by the red arrow in Fig. A.1), and the quartz tubes are then moved slowly into the cooling zone with a translation rate of about 0.2 mm/hr. We have monitored and measured the temperature profile of the cooling process versus the relative position of the sample using an R-type thermocouple, as displayed in Fig. A.1.

Acknowledgments

The STM work was supported by a grant from the U.S. Department of Energy (DOE), Office of Science (OS), Office of Basic Energy Sciences, under award No. DE-SC0014335. V.M. acknowledges partial support from Gordon and Betty Moore Foundation's EPIQS Initiative through grant GBMF4860. The ARPES work is supported by the U.S. Department of Energy (DOE), Office of Science (OS), Office of Basic Energy

Sciences, Division of Materials Science and Engineering, under Grant No. DE-FG02-07ER46383 (T-C.C.). This ARPES research used resources of the Advanced Light Source, which is a DOE Office of Science User Facility under contract No. DE-AC02-05CH11231. H.L. and R.S. acknowledge support from the Ministry of Science and Technology (MOST) in Taiwan, under Grant No. 109-2112-M-001-014-MY3 and Grant No. MOST-108-2112-M-001-049-MY2, respectively.

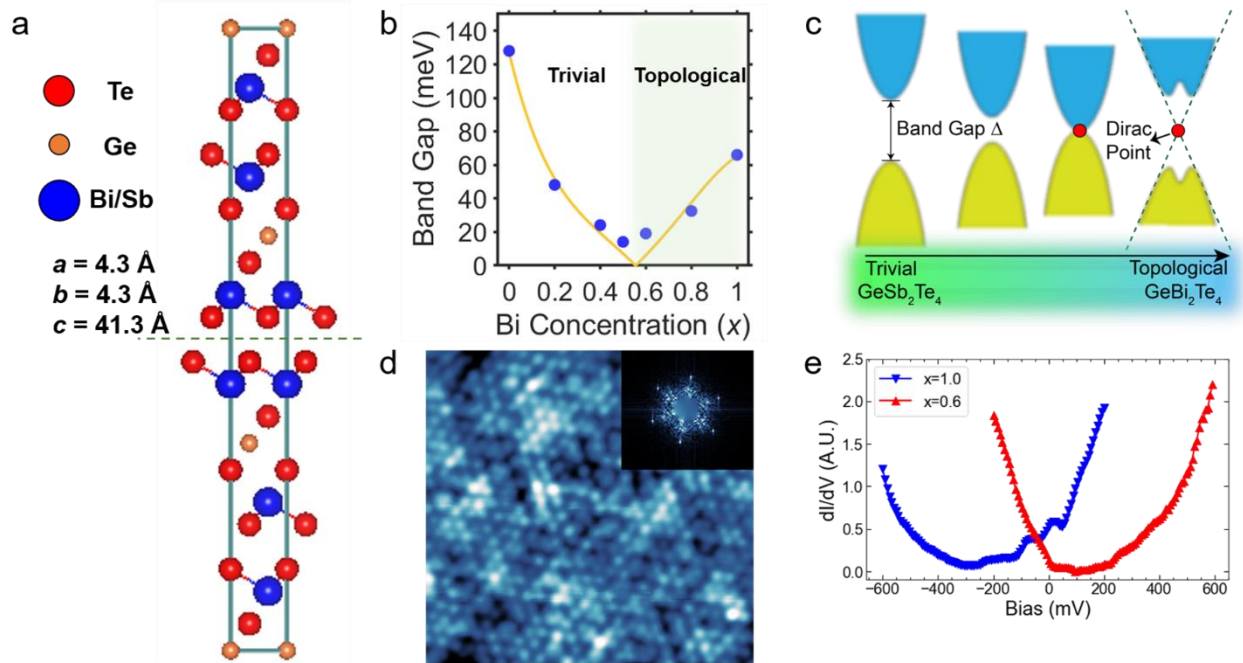


Figure 1 | Crystal Structure, DFT Predictions, STM Topography, and dI/dV Spectra. (a) Crystal structure of $\text{Ge}(\text{Bi}_x\text{Sb}_{1-x}/2)_2\text{Te}_4$; dashed line shows cleaving plane between two van der Waals bonded Te layers. (b) Density functional theory (DFT) calculated⁴ change in band gap with Bi doping leading to a trivial-to-topological phase transition. Figure from Singh, et al. (2013)⁴, with permission from authors. (c) Schematic of closing of bulk band gap with increased Bi substitution, followed by a reopening of the bulk gap and the appearance of linearly dispersing gapless topological surface states crossing at a Dirac point. (d) 10 nm \times 10 nm topography ($I_T = 450$ pA, $V_{\text{Bias}} = 100$ mV) of GeBi_2Te_4 showing a hexagonal lattice structure from the exposed Te surface; inset is the Fourier transform showing Bragg peaks. Topographies at each of the different substitutions are qualitatively very similar to each other. (e) dI/dV spectra for Bi substitutions of $x = 0.6$ and $x = 1.0$; the significant differences between the spectra suggest major changes in the band structure due to doping.

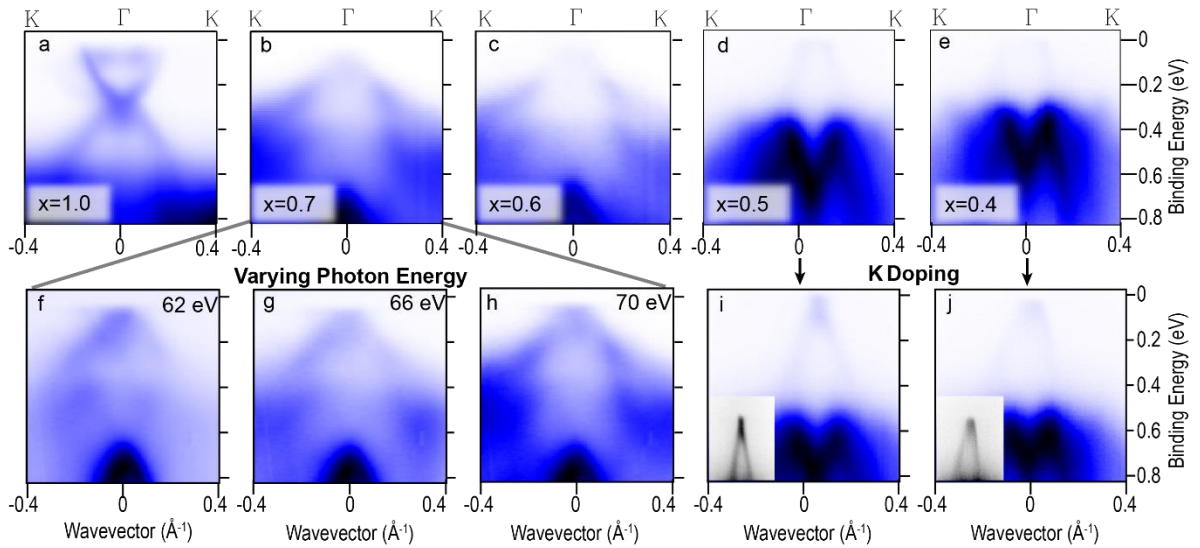


Fig. 2 | ARPES Measurements. (a)-(e) ARPES data along the Γ -K direction with different values of Bi doping x for $\text{Ge}(\text{Bi}_x\text{Sb}_{1-x})_2\text{Te}_4$. (f)-(h) $\text{GeBi}_{1.4}\text{Sb}_{0.6}\text{Te}_4$ ARPES spectra with varying incoming photon energy; the lack of change in the band structure confirms that the measured intensity is from 2D topological surface states. (i)-(j) ARPES measurements of potassium surface-doped samples with $x = 0.5$ and $x = 0.4$; K deposition shifts the Fermi level, making the Dirac point visible. Insets are close-ups of the spectra near the Dirac point.

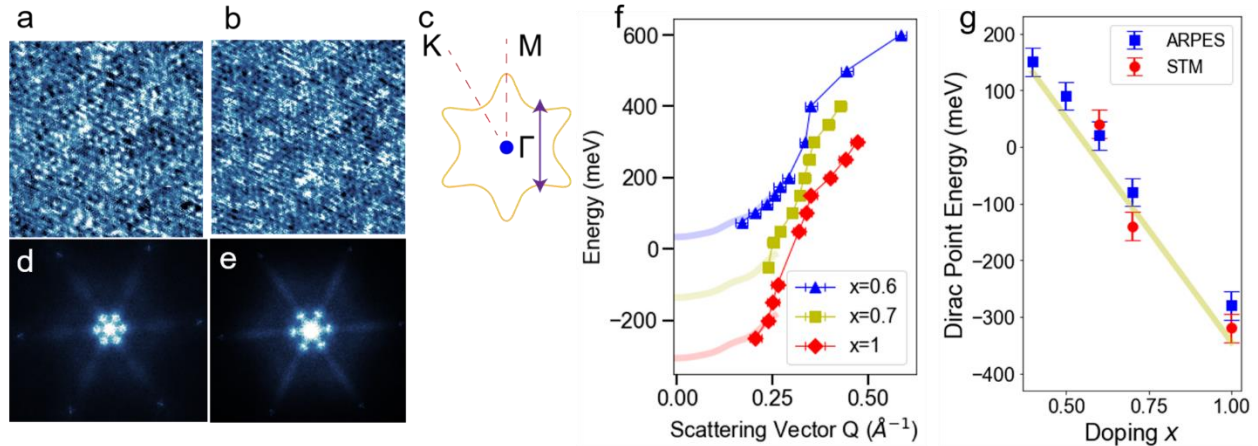


Fig. 3 | LDOS Maps, QPI, and Comparisons between FT-STs and ARPES. 60 nm \times 60 nm Local Density of States (LDOS) maps from STM dl/dV spectra on $\text{GeBi}_{1.4}\text{Sb}_{0.6}\text{Te}_4$ at (a) -50 meV and (b) 100 meV. (c) Schematic of hexagonally warped surface band structure; magenta arrow shows possible scattering vector along the Bragg peak Γ -M direction. (d)-(e) Fourier Transforms (FTs) of LDOS maps at -50 meV and 100 meV in (a)-(b). Quasiparticle interference (QPI) scattering vector \mathbf{q} , given by the peaks along the Γ -M direction, is larger at higher energy, indicating positive dispersion. Bragg peaks are faintly visible near the corners of the FTs. (f) QPI scattering dispersions from FTs of STM LDOS maps. Thick lines are extrapolations of dispersion line-shapes based on ARPES data in Fig. 2, allowing for determination of the Dirac points as 40 meV, -120 meV, and -320 meV for $\text{Ge}(\text{Bi}_x\text{Sb}_{1-x})_2\text{Te}_4$ doping values $x = 0.6$, $x = 0.7$, and $x = 1.0$, respectively. (g) Comparison of measured Dirac points shows overall agreement between QPI and ARPES findings, and an approximately linear relationship between the doping and the Dirac point energy.

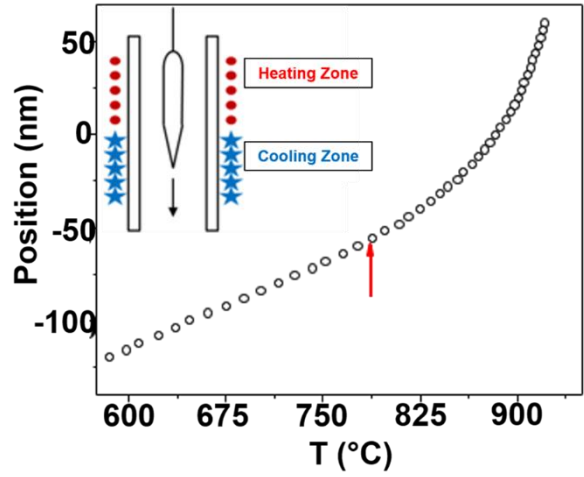


Figure A.1 | Single Crystal Growth. Temperature profile of the cooling process versus the relative position of sample. Inset shows a schematic of our vertical Bridgman furnace.

References

1. Qu, D., Hor, Y.S., Xiong, J., Cava, R.J. & Ong, N.P. Quantum oscillations and Hall anomaly of surface states in the topological insulator Bi₂Te₃. *Science*, **329** 821-824 (2010).
2. Hor, Y.S., Checkelsky, J.G., Qu, D., Ong, N.P. & Cava, R.J. Superconductivity and non-metallicity induced by doping the topological insulators Bi₂Se₃ and Bi₂Te₃. *J. Phys. Chem. Solids*, **72** 572-576 (2011).
3. Ghaemi, P., Mong, R.S.K. & Moore, J.E. In-plane transport and enhanced thermoelectric performance in thin films of the topological insulators Bi₂Te₃ and Bi₂Se₃. *Phys. Rev. Lett.*, **105** 166603 (2010).
4. Singh, B., Lin, H., Prasad, R. & Bansil, A. Topological phase transition and two-dimensional topological insulators in Ge-based thin films. *Phys. Rev. B*, **88** 195147 (2013).
5. Pesin, D. & MacDonald, A.H. Spintronics and pseudospintronics in graphene and topological insulators. *Nat. Mater.*, **11** 409-416 (2012).
6. Han, J., *et al.* Room-temperature spin-orbit torque switching induced by a topological insulator. *Phys. Rev. Lett.*, **119** 077702 (2017).
7. Kandala, A., *et al.* Growth and characterization of hybrid insulating ferromagnet-topological insulator heterostructure devices. *Appl. Phys. Lett.*, **103** 202409 (2013).
8. Checkelsky, J.G., Hor, Y.S., Cava, R.J. & Ong, N.P. Bulk band gap and surface state conduction observed in voltage tuned crystals of the topological insulator Bi₂Se₃. *Phys. Rev. Lett.*, **106** 196801 (2011).
9. Arakane, T. *et al.* Tunable Dirac cone in the topological insulator Bi_{2-x}Sb_xTe_{3-y}Se_y. *Nat. Commun.*, **3** 636 (2012).
10. Kong, D. *et al.* Ambipolar field effect in the ternary topological insulator (Bi_xSb_{1-x})₂Te₃ by composition tuning. *Nat. Nanotechnol.*, **6** 705-709 (2011).
11. Xu, S. *et al.* Topological phase transition and texture inversion in a tunable topological insulator. *Science*, **332** 560-564 (2011).
12. Ando, Y. Topological insulator materials. *J. Phys. Soc. Jpn.*, **82** 102001 (2013).
13. Neupane, M. *et al.* Topological surface states and Dirac point tuning in ternary topological insulators. *Phys. Rev. B* **85** 235406 (2012).
14. Schröder, T. *et al.* Thermoelectric properties of metastable Ge/Sb/Te and Ge/Bi/Te compounds. *AIP Conf. Proc.*, **1449** 159-162 (2012).
15. Siegrist, T. *et al.* Disorder-induced localization in crystalline phase-change materials. *Nat. Mater.*, **10** 202-208 (2011).
16. Matsunaga, T. & Yamada, N. Structural investigation of GeSb₂Te₄: a high-speed phase-change material. *Phys. Rev. B*, **69** 104111 (2004).
17. Okamoto, K. *et al.* Observation of a highly spin-polarized topological surface state in GeBi₂Te₄. *Phys. Rev. B*, **86** 195304 (2012).
18. Hoffman, J.E. Spectroscopic scanning tunneling microscopy insights into Fe-based superconductors. *Rep. Prog. Phys.*, **74** 124513 (2011).

19. Wang, Z., Chong, Y., Joannopoulos, J.D. & Soljačić, M. Observation of unidirectional backscattering-immune topological electromagnetic states. *Nature*, **461** 772-776 (2009).
20. Beidenkopf, H. *et al.* Spatial fluctuations of helical Dirac fermions on the surface of topological insulators. *Nat. Phys.*, **7** 939-943 (2011).
21. Arita, M. *et al.* Angle resolved photoemission study of GeBi₂Te₄. *JPS Conf. Proc.*, **1** 012017 (2014).
22. Cava, R.J., Ji, H., Fucillo, M.K., Gibson, Q.D. & Hor, Y.S. Crystal structure and chemistry of topological insulators. *J. Mater. Chem. C*, **1** 3176-3189 (2013).
23. Wang, J. *et al.* Genesis and effects of swapping bilayers in hexagonal GeSb₂Te₄. *Chem. Mater.*, **30** 4770-4777 (2018).
24. Shelimova, L.E. *et al.* X-Ray diffraction study and electrical and thermal transport properties of the *n*GeTe-*m*Bi₂Te₃ homologous series compounds. *J. Alloys Compd.*, **329** 50-62 (2001).
25. Gyenis, A. *et al.* Quasiparticle interference on the surface of the topological crystalline insulator Pb_{1-x}Sn_xSe. *Phys. Rev. B*, **86** 125414 (2013).
26. Okada, Y. *et al.* Visualizing Landau levels of Dirac electronics in a one-dimensional potential. *Phys. Rev. Lett.*, **109** 166407 (2012).